



The Development of Mn Doped NiO@RGO Nanocomposite for Supercapacitors Applications

Yared S. Worku *, Ludwe L. Sikeyi, Nithyadharseni Palaniyandy, Mkhulu M. Mathe

Institute for the Catalysis and Energy Solutions (ICES), College of Science and Engineering, Technology, University of South Africa, Florida Science Campus, Roodepoort 1709, South Africa.

Corresponding author email: yared76@yahoo.com

ABSTRACT:

NiO is a potentially electroactive material for energy storage applications. However, its poor electrical conductivity and low ionic transport properties have restricted its potential for supercapacitor applications. To overcome the problems doping with metal elements and making RGO composite is a possible solution to improve the electrochemical performance of NiO. In this study Mn-doped NiO@RGO nano-composite materials were synthesized via a co-precipitation followed by hydrothermal method this method is advantages to control particle size and produce high purity sample. The result showed that doping of Mn and integration of RGO with NiO improved the specific capacity of NiO from 514 F g^{-1} to 1870 F g^{-1} at 1.0 A g^{-1} and increased its cycle stability from 80.7% to 90% over 1000 cycles. Moreover, Mn-NiO@RGO showed a higher energy density of $63.05 \text{ Wh (Kg)}^{-1}$ at $285.4 \text{ W (Kg)}^{-1}$, compared to Mn-NiO and NiO. Therefore, the Mn doped NiO@RGO electrode could be a promising material for advanced energy storage systems.

Key words: Supercapacitor, Mn-NiO@RGO , Co-precipitation, Hydrothermal, Specific capacity

1. INTRODUCTION

The continuous use and consumption of fossil fuels produce harmful air pollutants to the atmosphere, which causes global warming and destruct ecosystems to rise. Therefore, scientists have explored alternative renewable energy sources that do not affect the natural eco system [1]. However, as the world increasingly depends on renewable energy sources, there must be a technologies that is capable of storing these energy [2]. Energy storage is essential in order to maintain a steady stream of sustainable energy for power grids. Batteries and Supercapacitors (SCs) are essential electrochemical energy storage (EES) devices due to their affordability and widespread range of capabilities. Although batteries are necessary that require constant power and high energy density, they have short lifespans and low power densities as compared to SCs [3]. SCs have high power density, fast to charge and discharge, low maintenance requirements, extended life-span, and eco-friendliness. However, SC still have limited energy density compared to batteries, affecting their widespread applications in various industries [4]. Therefore, there is a significant push in current research efforts to enhance SCs with increased energy and power densities for their potential as main power sources [5]. Based on the charge storage mechanism SCs are classified into electrical double-layer capacitors (EDLCs), which store energy based on ion absorption/desorption, and pseudo-capacitors use fast surface redox reactions [6]. Carbon-based materials are commonly used for EDLC, whereas conducting polymers and transition metal oxides are well known pseudo-capacitive materials [6]. Among transition metal oxides, NiO is the most studied pseudo-capacitive electrode materials due to its high theoretical capacitance (2584 F g^{-1}), low price, low toxicity, and easy to synthesize [7]. However, its poor electrical conductivity and low ionic transport has restricted its potential for SCs. Recently various techniques have been applied such as doping, introducing oxygen vacancies, and making composites with carbon materials to improve the electrochemical performance of NiO materials, doping with metal elements providing more active sites, increased stability, and improved electrical conductivity of NiO. Moreover, making composite with carbon materials minimizes aggregation and improves the electrical conductivity of NiO [8]. For instance. Shyamali et al synthesized Co doped NiO combustion route method. Co-NiO exhibited a maximum specific capacity of 1244 F g^{-1} which is far superior to undoped NiO (295 C/g) and 83.7 % of initial capacity even after 5000 cycles [9]. Han et al. studied manganese-doped nickel oxide using a hydrothermal process. Their electrochemical analysis showed that the doped material has a capacitance retention of 75% and a Cs of 1166 F g^{-1} . Sivakumar et al. studied Mn doped NiO nanoparticles for supercapacitor application [10]. Han et al. studied the inductive effect in arrays of Mn-doped NiO nanosheets. They discovered that Mn-doped NiO nanosheets achieved higher specific capacitance than pure NiO nanosheet [11]. Srikesk et al. studied the electrochemical performance of Co and Mn doping NiO. The doped NiO exhibited superior specific capacitance of 673.73 F g^{-1} and high electrochemical cyclic stability than pure NiO [12]. Alharbi et al. developed Mn doped NiO@RGO using hydrothermal method. Mn doped NiO@rGO achieved exceptional high specific capacitance (Cs) of 1780.32 F g^{-1} at 1.0 A g^{-1} , and capacity retention of 96% over 6000 cycles [13]. This study investigated the electrochemical properties of Mn-doped NiO in combination with RGO to form Mn-NiO@RGO nanocomposite. This type of design is advantageous for boosting electrical conductivity, improving specific capacity and cyclic stability of NiO

2. Experimental section

2.1. Synthesis of NiO, Mn-NiO and Mn-NiO@RGO.

NiO and Mn-NiO nano particles

In this work, 0.2 M Ni (NO₃)₂·6H₂O, and 0.04 M C₆H₈O₇ were dissolved in 60 mL of distilled water (Dw) with continuous stirring for 30 minutes. In addition, 0.1 M NaOH was added to the solution to maintain the pH value to be 12. While being agitated constantly on a magnetic stirrer at 80 °C for one hour, the solution eventually transformed into a green solid. The product was washed with acetone to eliminate any organic or undesired impurities and unwanted reactants. The entire mixture was placed in a microwave and heated to 110 °C for 5 hours. The final product was heated at 900 °C for 5 hours in furnace. The mortar and pestle were used to crush all the samples into a (NiO) fine powder. For Mn-NiO we used similar methods with NiO except we used 0.04 M Mn(NO₃)₂·6H₂O as a starting material.

Mn-NiO@RGO nanocomposite

For Mn-NiO@RGO we use hydrothermal approach for the formation of supercapacitor electrodes. It is inexpensive, simple and eco-friendly. First 200 mg of RGO and 200 mg of Mn-doped NiO in a 1:1 ratio was added in a 50 mL of distilled water (Dw), and then the mixture was stirred with a magnetic stirrer for 50 minutes. The solution was transferred into 50ml Teflon for hydrothermal reaction subjected to heating at a temperature of 180 °C for 8 hours. Following the treatment, the final product was washed several times with Dw in a centrifuge to eliminate any impurity before drying in a vacuum at 80 °C.

2.2 Electrode fabrication

The electrode material was fabricated by mixing 7 mg of the active materials (NiO, Mn-NiO and Mn-NiO@RGO), polyvinylidene fluoride (PVDF), and super P in the ratio of (8:1:1) in a mortar and grinding until it becomes a homogeneous mixture followed by subjecting it to ultrasonic treatment for 30 minutes to form slurry. The slurry was then pasted with a drop casting on carbon cloth (1x1cm²) with a micropipette and then placed in an electric oven to dry.

3. Electrochemical analysis characterization

The electrochemical performance of all the fabricated electrodes were characterized using cyclic voltammetry (CV), galvanostatic charge–discharge (GCD) and electrochemical impedance spectroscopy (EIS) in a three-electrode system in 2.0 M KOH electrolyte solution. From CV curve the specific capacitance (C_s) can be calculated using Eqn. 1.

$$C_s = \frac{\int IdV}{V_s \times \Delta V \times m} \quad (1)$$

Where $\int IdV$ is the area under CV curve, V_s is the scan rate, ΔV is the potential window, and m is the total mass of active material loaded on the carbon cloth. The energy density (E_d) and power density (P_d) can be calculated using Eqn. 2 and Eqn. 3 below.

$$E_d = \frac{C_s \Delta V^2}{7.2} \quad (2)$$

$$P_d = \frac{(C_s \Delta V V_s)}{7200} \quad (3)$$

From the GCD graph C_s can be calculated

$$C_s = \frac{I \Delta t}{m \Delta V} \quad (4)$$

Where Δt is the discharge time using Eqn.2, 3 and Eqn.4, the P_d can be determined as

$$P_d = \frac{E_d \times 3600}{\Delta t} \quad (5)$$

4. Results and Discussion

4.1. XRD Analysis

Fig. 1(a) illustrates the XRD peaks of NiO, Mn-NiO and Mn-NiO@RGO. The typical peaks of NiO are positioned at a specific angle of 2-Theta (θ) corresponding to the crystal planes. By referring to JCPDS card 73-1523, all peaks in crystallography have been recognized as belonging to the face-centered cubic phase. However, no peaks associated with MnO appeared, indicating that Mn-NiO was successfully prepared. Mn-NiO exhibited the same XRD pattern as NiO, and the small peaks found at 26° in Mn-NiO@RGO confirmed the existence of RGO, indicating that the Mn-NiO@RGO nanocomposite was successfully formed.

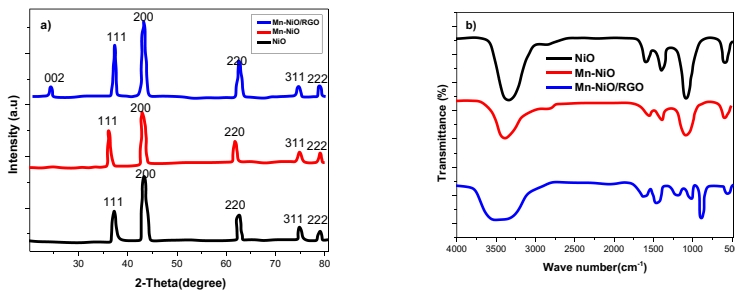


Fig. 1 (a) XRD pattern (b) FTIR spectrum of Mn-NiO and Mn-NiO@RGO.

4.2. FTIR Analysis

Fig. 1(b) displays the FTIR spectra of NiO, Mn-NiO and Mn-NiO@RGO nanoparticles within the range of 500 to 4000 cm^{-1} wave-number. The 3400 cm^{-1} peak is attributed to the O-H stretching vibration of interlayer H_2O molecules, while the 1637 cm^{-1} peak is due to the bending vibrations of H-O-H molecules. The transmittance bands at 1529.5 , 1342 , and 1016 cm^{-1} represent the OH band, and the 523.2 cm^{-1} band is related to Ni-O. As a result, the Mn doped NiO shows NiO peaks and a slight shift in bands, indicating the formation of Mn doped NiO [14]. The different peaks

appeared at 1403.6, 1150.3, and 833.7 cm^{-1} are attributed to C=O, C=C, and C–O stretching, confirming the presence of RGO in Mn-NiO@RGO. The FTIR analysis confirms the successful synthesis of Mn-NiO@RGO nanocomposites.

SEM and EDS Analysis

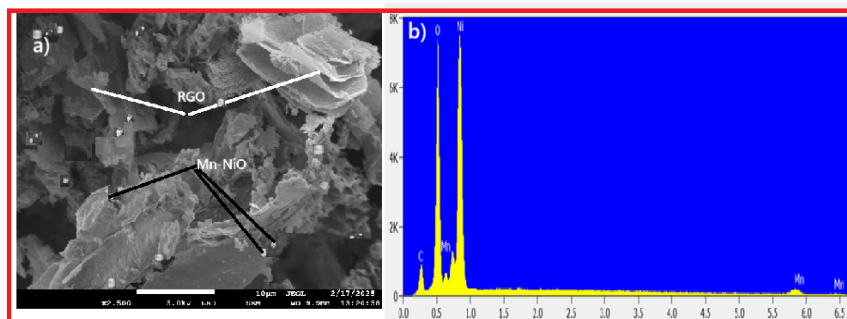


Fig. 2. a) high magnification of SEM images b) EDS of Mn-NiO@RGO nanocomposites.

Fig. 2(a) showed the typical SEM images of synthesized Mn-NiO@RGO nanocomposites. The nanoparticles on the RGO's surface show that the Mn-NiO nanoparticles have been successfully integrated into the RGO sheets, resulting in the sheets cracking in some places and exhibiting some agglomeration of nanoparticles. The different elements in Mn-NiO@RGO are displayed in their composition by the EDS spectra in Fig. 2(b).

4.3 Electrochemical Analysis.

From CV curve we can understand that as the scan rate increases the CV curve shows symmetrical and its shape remains consistent demonstrating that the fabricated electrode materials have excellent kinetic reversibility, high-rate capability Fig 3 (a, b, c). The presence of peaks for oxidation and reduction indicates a pseudo-capacitive nature of materials. By using equation (1), the C_s values are 651.6, 689.6 and 1670.8, F g^{-1} at scan rates of 5mV s^{-1} for NiO, Mn-NiO and Mn-NiO@RGO, respectively. This shows that the doping of Mn in NiO facilitates the creation of oxygen vacancies (O vacancies). These vacancies act as active sites for electrochemical reactions, increasing the material's capacity to store and release ion [15]. Incorporating RGO into Mn-NiO enhances specific capacity due to the synergistic effects of RGO's high conductivity and large surface area, which improve electron transfer and ion diffusion, respectively, leading to enhanced electrochemical performance [16]. From fig. 3(c) the increased C_s value for Mn-NiO@RGO is attributed to the addition of a Mn into NiO that generates an oxygen vacancy and offers more active sites necessary for the electrolyte ion adsorption and improves the charge transfer kinetics for supercapacitor applications.

From the galvanostatic charge/discharge (GCD) graph all the materials show symmetrical triangular (nonlinear) charging/discharging curves without considerable internal resistance (Fig. 3(d, e, f)), which is consistent with the expected pseudo-capacitance behavior of materials [17]. The GCD result further studies the C_s of the fabricated

materials using Eqn. 4 and the calculated C_s are 514, 320, 178.5 and 89.8 $F g^{-1}$ for NiO, 731,448, 251 and 137 $F g^{-1}$ for Mn-NiO and 1817, 1074, 621, 315 $F g^{-1}$ for Mn-NiO@RGO at 1A g^{-1} . The calculated C_s value showed that large capacitive were found in Mn-NiO@RGO (Fig. 3(f)). Moreover Mn-NiO@RGO possesses higher discharging rate compared to others which is like CV measurements. At low current density, the GCD curves show a delay in charging / discharging because of minimal electrolyte ion diffusion within the electrode materials' surface area. However, at higher currents, the electrolyte ions are limited to passing the interface and engaging with the electrodes' interfacial sites leads to fast charge/discharge time (Fig. 3(d, e, f)). Table 1 shows the comparative results of our prepared Mn-NiO@RGO with other reported in literature.

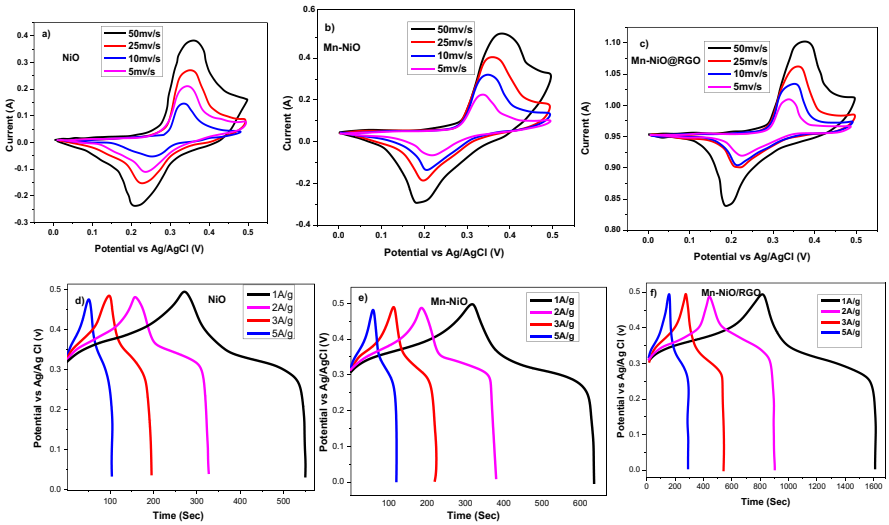


Fig. 3 CV plot of a) NiO, b) Mn-NiO, c) Mn-NiO@RGO. GCD plot of d) NiO, e) Mn-NiO, f) Mn-NiO@RGO.

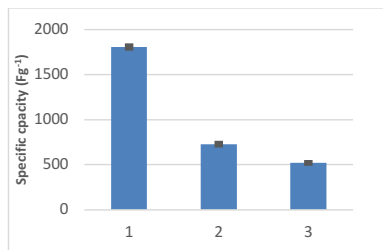


Fig. 4 Bar height and error bars of specific capacitance for the average and standard deviation of 1) Mn-NiO@RGO 2) Mn-NiO and 3) NiO at 1 A g⁻¹

The results are shown in Fig. 4(d-f) for the current density (1 Ag⁻¹, 2 A g⁻¹ and 3 A g⁻¹), the Mn-NiO@RGO electrode produced higher specific capacity. To indicate the variability or uncertainty of our reported measurement, we used standard deviation and standard error. A summary of the specific capacitance averages and standard deviations at 1Ag⁻¹ are shown in the bar graphs in Fig. 3. At 1 Ag⁻¹, the Mn-NiO@RGO, Mn-NiO and NiO electrodes exhibited specific capacitances of 1806.75 ± 13,55 F g⁻¹, 729,25 ± 10,10, F g⁻¹ and 521,25 ± 4,96 F g⁻¹ respectively.

The EIS analysis was conducted to determine the internal resistance between the electrode and the electrolyte. Fig. 5(a) shows the Nyquist plots for the fabricated materials. Both Mn-NiO and NiO materials displays a semi-circle in the low-frequency region due to the charge transfer impedance at the electrode-electrolyte interface, while the ideal capacitive behavior is indicated by the straight line [18]. However, Mn-NiO@RGO lacks the semicircle region in high frequency, possibly because of the decreased faradic resistance [13]. Mn-NiO@RGO displays a semi-circle arc in the low-frequency range compared to other materials indicating a more rapid internal ion diffusion rate, indicating a quicker internal ion diffusion speed. From EIS graph the electron transfer resistance of Mn-NiO@RGO is (0.9 Ω, which is higher than that of Mn-NiO (1.14 Ω) and NiO (1.7 Ω). These findings indicate that the Mn-NiO@RGO possess high internal electron transport speed compared to the other fabricated materials.

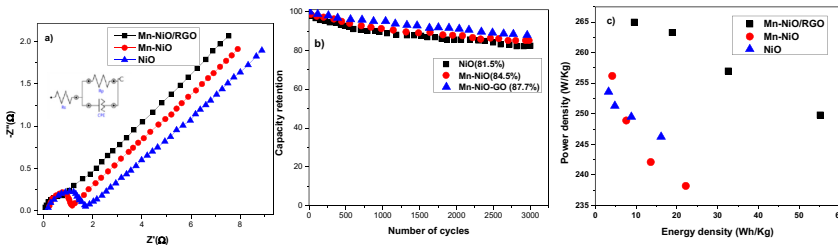


Fig. 5 a) EIS spectra, b) Cycle stability at 5 mv s⁻¹, c) Ragone plot of NiO, Mn-NiO and Mn-NiO@RGO.

The cycling stability is one of the most important factors for supercapacitor material. As shown in Fig. 5(b) Mn-NiO@RGO (90%) has higher stability than both Mn-NiO (84%) and NiO (80.7%) over 1000 cycles. Additionally, the Ragone plot (Fig. 5(c)) is used to examine the relationship between the electrode material's energy density (E_d) and P_d using Eqn. 5 and 6. the calculated E_d value is 18.44 , 25.37, 63.05 Wh (Kg)⁻¹ and P_d is 281.4 ,283.6 and 285.4 W (Kg)⁻¹ at 1 A g⁻¹ for NiO, Mn- NiO and Mn-NiO@RGO, respectively .The findings indicate that the value of E_d is less than E_p and Mn-NiO@RGO materials possess highest energy density than other.

Table 1. Comparative electrochemical analysis of NiO based materials

| Samples | Electrolyte | substrate | Current density (A g ⁻¹) | Specific capacity (F g ⁻¹) | Cyclic stability | Ref |
|------------|---------------------------------|----------------|--------------------------------------|--|--------------------------|-----------|
| Zn-Mn-NiO | Na ₂ SO ₄ | Nickel foam | 0.2 | 313 | - | [19] |
| Mn-NiO | KOH | graphite sheet | 0.5 | 369.6 | 96.5% over 10,000 cycles | [20] |
| NiO@RGO | KOH | Nickel foam | 0.38 | 428 | 90.2% over 5000 cycles | [21] |
| Mn-NiO@RGO | KOH | Nickel foam | 1 | 1780 | 96% over 6000 cycles | [13] |
| Mn-NiO@RGO | KOH | Carbon cloth | 1 | 1817 | 87.3% over 3000 cycles | This work |

Conclusion

To summarize, Mn-doped NiO@RGO was prepared via co-precipitation followed by hydrothermal method. Doping of Mn to Mn-NiO creates additional electrochemical active sites, enhancing electrochemical activity and the formation of nano-composite with RGO decreases the distance for electrolyte ion diffusion and electron transfer resistance (0.92 Ω) which led to a superior redox process. The developed Mn-NiO@RGO nano-composite exhibited excellent specific capacity of 1817 F g⁻¹, high energy density of 63.05 Wh (Kg)⁻¹ at 285.4 W (Kg)⁻¹ at 1.0 A g⁻¹. Moreover, the fabricated nanocomposite achieved high cyclic stability of 90% after 1000 cycles. This shows the developed Mn-NiO@RGO nanocomposite provides a novel approach for enhancing the performance of energy storage devices.

Declaration of Competing Interest

The authors declare no conflicts of interest.

Acknowledgment

The authors would like to thank the University of South Africa (UNISA) for the facility and providing financial support.

Reference

1. Wang, J. and W. Azam, *Natural resource scarcity, fossil fuel energy consumption, and total greenhouse gas emissions in top emitting countries*. *Geoscience Frontiers*, 2024. **15**(2): p. 101757.
2. Sayed, E.T., et al., *Renewable energy and energy storage systems*. *Energies*, 2023. **16**(3): p. 1415.
3. Mitali, J., S. Dhinakaran, and A. Mohamad, *Energy storage systems: A review*. *Energy Storage and Saving*, 2022. **1**(3): p. 166-216.
4. Kularatna, N. and K. Gunawardane, *Energy storage devices for renewable energy-based systems: rechargeable batteries and supercapacitors*. 2021: Academic Press.

5. Sharma, S. and P. Chand, *Supercapacitor and electrochemical techniques: A brief review*. Results in Chemistry, 2023. **5**: p. 100885.
6. Olabi, A.G., et al., *Carbon-based materials for supercapacitors: recent progress, challenges and barriers*. Batteries, 2022. **9**(1): p. 19.
7. Meng, T., et al., *The electrochemical capacitive behaviors of NiO nanoparticles*. Electrochimica Acta, 2014. **125**: p. 586-592.
8. Kate, R.S., S.A. Khalate, and R.J. Deokate, *Overview of nanostructured metal oxides and pure nickel oxide (NiO) electrodes for supercapacitors: A review*. Journal of Alloys and Compounds, 2018. **734**: p. 89-111.
9. Vazhayil, A., J. Thomas, and N. Thomas, *Enhanced electrochemical performance of facilely synthesized cobalt doped cubic NiO nanoflakes for supercapacitor application*. Journal of Energy Storage, 2022. **55**: p. 105498.
10. Sivakumar, S. and N.A. Mala, *Synthesis and characterization of manganese doping on NiO nanoparticles and its supercapacitor applications*. Materials Today: Proceedings, 2022. **49**: p. 1469-1474.
11. Han, X., et al., *Inductive effect in Mn-doped NiO nanosheet arrays for enhanced capacitive and highly stable hybrid supercapacitor*. ACS Applied Energy Materials, 2019. **2**(3): p. 2072-2079.
12. Srikesh, G. and A.S. Nesaraj, *Chemical synthesis of Co and Mn co-doped NiO nanocrystalline materials as high-performance electrode materials for potential application in supercapacitors*. Ceramics International, 2016. **42**(4): p. 5001-5010.
13. Alharbi, F., et al., *Facile development of Mn doped NiO nanoarrays supported on a reduced graphene oxide nanocomposite as a supercapacitor*. Energy & Fuels, 2023. **37**(16): p. 12225-12235.
14. Mala, N.A., et al., *Supercapacitor and magnetic properties of NiO and manganese-doped NiO nanoparticles synthesized by chemical precipitation method*. Journal of Materials Science: Materials in Electronics, 2023. **34**(6): p. 505.
15. Gao, P., et al., *The role of cation vacancies in electrode materials for enhanced electrochemical energy storage: synthesis, advanced characterization, and fundamentals*. Advanced Energy Materials, 2020. **10**(14): p. 1903780.
16. Singh, M.K., et al., *Effective assembling of nickel oxide-reduced graphene oxide heterostructures for ultrahigh capacity supercapattery*. Journal of Power Sources, 2024. **595**: p. 234060.
17. Bhojane, P., *Recent advances and fundamentals of Pseudocapacitors: Materials, mechanism, and its understanding*. Journal of Energy Storage, 2022. **45**: p. 103654.
18. Sunil, V., et al., *Characterization of supercapacitive charge storage device using electrochemical impedance spectroscopy*. Materials Today: Proceedings, 2021. **46**: p. 1588-1594.
19. Mala, N.A., et al., *Enhanced electrochemical properties of zinc and manganese co-doped NiO nanostructures for its high-performance supercapacitor applications*. Inorganic Chemistry Communications, 2022. **142**: p. 109661.
20. Srikesh, G. and A.S. Nesaraj, *Facile preparation and characterization of novel manganese doped nickel oxide based nanostructured electrode materials for application in electrochemical supercapacitors*. Journal of Asian Ceramic Societies, 2020. **8**(3): p. 835-847.
21. Li, W., et al., *The preparation of hierarchical flowerlike NiO/reduced graphene oxide composites for high performance supercapacitor applications*. Energy & fuels, 2013. **27**(10): p. 6304-6310.

Open Access This chapter is licensed under the terms of the Creative Commons Attribution-NonCommercial 4.0 International License (<http://creativecommons.org/licenses/by-nc/4.0/>), which permits any noncommercial use, sharing, adaptation, distribution and reproduction in any medium or format, as long as you give appropriate credit to the original author(s) and the source, provide a link to the Creative Commons license and indicate if changes were made.

The images or other third party material in this chapter are included in the chapter's Creative Commons license, unless indicated otherwise in a credit line to the material. If material is not included in the chapter's Creative Commons license and your intended use is not permitted by statutory regulation or exceeds the permitted use, you will need to obtain permission directly from the copyright holder.

